The Ground State of Epitaxial Germanene on Ag(111)

Kai Zhang, Marie-Christine Hanf, Romain Bernard, Yves Borensztein, Hervé Cruguel, Andrea Resta, Yves Garreau, Alina Vlad, Alessandro Coati, Davide Sciacca, et al.

The ground state of epitaxial germanene on Ag(111)

K. Zhang,[#] M.-C. Hanf,[&§] R. Bernard,[#] Y. Borensztein,[#] H. Cruguel,[#] A. Resta,[♦] Y. Garreau,[♦‡] A. Vlad,[♦] A. Coati,[♦] D. Sciacca,[†] B. Grandidier,[†] M. Derivaz,[&§] C. Pirri,[&§] P. Sonnet,[&§] R. Stephan,[&§] G. Prévot[#]*

[#] Sorbonne Université, Centre National de la Recherche Scientifique, Institut des NanoSciences de Paris, INSP, F-75005 Paris, France

[&] Université de Haute Alsace, CNRS, IS2M UMR7361, F-68100 Mulhouse, France

[§] Université de Strasbourg, France

[♦] Synchrotron SOLEIL, L'Orme des Merisiers Saint-Aubin, BP 48 91192 Gif-sur-Yvette Cedex, France

[‡] Université Paris Cité, Laboratoire Matériaux et Phénomènes Quantiques, CNRS, F-75013, Paris, France

[†] Univ. Lille, CNRS, Centrale Lille, Univ. Polytechnique Hauts-de-France, Junia-ISEN, UMR 8520 - IEMN, F-59000 Lille, France

KEYWORDS.

Germanene, Silver, Scanning tunneling microscopy, Surface x-ray diffraction, Density functional theory.

ABSTRACT.

Two-dimensional (2D) honeycomb lattices beyond graphene, such as germanene, appear very promising due to their outstanding electronic properties, such as quantum spin hall effect. While there have been many claims of germanene monolayers up to now, no experimental evidence of a honeycomb structure has been given up to now for these grown monolayers. Using scanning tunneling microscopy (STM), surface X-ray diffraction (SXRD) and density functional theory, we have elucidated the Ge-induced $\left(\sqrt{109} \times \sqrt{109}\right)R \pm 24.5°$ reconstruction on Ag(111). We demonstrate that a powerful algorithm combining SXRD with STM allows us to solve a giant surface reconstruction with more than hundred atoms per unit cell. Its extensive unit cell indeed consists of 98 two-fold or three-fold coordinated Ge atoms, forming a periodic arrangement of pentagons, hexagons and heptagons, with the inclusion of 6 dispersed Ag atoms. By analogy, we show that the $\left(7\sqrt{7} \times 7\sqrt{7}\right)R \pm 19.1°$ reconstruction obtained by segregation of Ge through an epitaxial Ag/Ge(111) film possesses a similar structure, i.e. Ge pentagons/hexagons/heptagons with a few Ag atoms. Such an organization is more stable than pure Ge monolayers and can be assigned to the ground state of epitaxial germanene.

Following the graphene discovery, the synthesis of other monoelemental honeycomb lattices, known as xenes,[1,2] has been widely reported. In particular, silicene, germanene, stanene, plumbene, which, together with graphene, form the group-IVA xenes, possess similar electronic properties as graphene, with however a stronger spin-orbit coupling (SOC), resulting in a larger gap in the electronic structure at the Fermi level. With a predicted SOC of 24 meV,[3] and with an easy integration into current electronic devices, germanene is thus considered as a promising material for quantum spin Hall effect observations and technological applications in spintronics.[4]

The synthesis of epitaxial germanene has been first reported in 2014 on Pt(111).[5] After room temperature deposition of 1 ML of germanium followed by annealing at 600–750 K for 30 min, a $\left(\sqrt{19} \times \sqrt{19}\right)R23.4°$ reconstruction is observed by low energy electron diffraction (LEED) and STM and attributed to honeycomb epitaxial germanene. Following this pioneering work, germanene synthesis has been reported on various substrates, such as GePt,[6] Au(111)[7], Al(111)[8], MoS_2,[9] HOPG,[10] Sb(111),[11] Cu(111),[12] or Ag(111).[13] However, these findings have been questioned and the formation of surface germanides has been also proposed in the case of Ge/Pt(111),[14] Ge/Ag(111),[15,16] Ge/Au(111),[17–19] and Ge/Al(111).[20–22] In particular, we have demonstrated that Ge deposited on Al(111) form surface or two-layer alloys.[21,22] Germanene formation at the surface of HOPG has also been refuted,[23] while the possibility of germanium intercalation between MoS_2 layers has been raised. Thus, the demonstration of the existence of honeycomb germanene is still under debate.

Among all these systems, Ag(111) which is known to be well suited for the growth of silicene,[2] appeared as the best substrate for germanene synthesis and is undoubtedly the most discussed one today. The first ordered structure observed after Ge growth in the 300 K – 600 K

temperature range is a $(\sqrt{3} \times \sqrt{3})R30°$ reconstruction, attributed to a Ag_2Ge surface alloy.[15,24,25] A more precise analysis has shown that this reconstruction has a larger superstructure and form stripes running along the <112> directions of the Ag(111) surface.[26] The precise periodicity of the striped pattern depends on the preparation conditions, since several unit cells have been reported.[13,26–31] On the basis of scanning tunneling microscopy (STM), some authors have proposed that this stripe pattern corresponds to a pure germanene layer, highly distorted with respect to free-standing germanene.[13,30] However, our recent surface X-ray diffraction measurements demonstrate that the stripe pattern corresponds to a Ag_2Ge surface alloy with an atomic density 6.45% higher than the Ag(111) atomic density. The overall structure is formed by stripes associated with a face-centered cubic top-layer alignment, alternating with stripes associated with a hexagonal-close-packed top-layer alignment, in great analogy with the $(22 \times \sqrt{3})$ Au(111) reconstruction.[29]

For increasing germanium coverage θ_{Ge}, the stripe pattern is replaced by a disordered hexagonal (DH) structure,[13,16,30] associated with an apparent $c(\sqrt{3} \times 7)$ reconstruction.[31,32] It has been described either as a germanene layer,[13,30,31] or as a $AgGe_2$ surface alloy.[16] Further increase of the Ge coverage results in the formation of protrusions which assemble into dimers, trimers, tetramers, and hexamers on the surface.[28] These protrusions have been assigned to Ge adatoms on a Ag_2Ge surface alloy.[28,33] Similar features have been observed after annealing, at 753K, a thick Ag film grown on Ge(111).[34,35] Moreover, the sequence of structures observed during growth around 600 K is reproduced by the Ge segregation method when increasing the annealing temperature from 630 K to 750 K,[35] confirming the increasing Ge coverage for the stripe, DH and hexamer/dimer structures respectively. For the higher temperature of segregation, the surface exhibits a $(7\sqrt{7} \times 7\sqrt{7})R19.1°$ reconstruction composed of one hexamer and three dimers per

unit cell.[34] It is also described as a $\left(3\sqrt{21} \times 3\sqrt{21}\right)R10.9°$ reconstruction of a honeycomb germanium layer, with a lattice constant of 0.39 nm, i.e., very close to the one of free-standing germanene (0.397 nm).[36] However, the ball-and-stick model proposed corresponds in reality to a smaller unit cell, namely a (7×7) one with respect to the Ag substrate, which consequently cannot account for the STM observation. Moreover, no additional theoretical support has been given up to now to test the validity of this ball-and-stick model.

As concerns the electronic structure of the grown layers, a good agreement was found between Angle-resolved photoemission spectroscopy (ARPES) measurements and DFT computation of the band structure that clearly points to the existence of a surface Ag_2Ge surface alloy at low coverage.[24] On the contrary, a less good agreement is found when comparing ARPES measurements performed on the striped phase with a model of tensile strained germanene on Ag(111).[13] Finally, the weak signal observed by ARPES for the DH phase has been interpreted as originating from free-standing germanene,[13] but it is probable that the Ag substrate should strongly modify the electronic structure of germanene, such as what is observed for silicene.[2]

The lack of precision of germanene coverage in the previous experiments, the assignment to a germanene layer given for a large variety of structures observed sequentially during growth and having obviously a different Ge coverage made the situation incomprehensible. In this paper, using STM, surface X-ray diffraction (SXRD) and density functional theory (DFT), we determine the atomic structure of the hexamer phase and show that it corresponds to a 2D plane of Ge atoms, organized in hexagons, pentagons and heptagons, without four-fold coordinated Ge atoms and with a very small amount of Ag atoms. We show that such structure is thermodynamically more stable than a pure Ge layer. As such configuration is obtained both

from the segregation and from the evaporation of Ge atoms, it can be considered as the ground state of epitaxial germanene.

RESULTS AND DISCUSSION

After depositing 0.9±0.1 ML Ge on Ag(111) at 455K, the surface is homogeneously covered with the reconstruction shown in the STM image in Fig. 1a. Here, 1 ML corresponds to the density of a honeycomb Ge layer with lattice constant 0.397 nm. This reconstruction displays a pattern of 6-petal flowers (hexamers), with a hexagonal unit-cell, and two domain orientations. The size of the unit cell is 3.0 x 3.0 nm^2, and the two domains are rotated by ±25° from the <110> axes of the Ag surface. The pattern looks similar to the one shown in the supplemental information of ref. [28]. This reconstruction is observed if deposition is performed in the 400 K – 460 K temperature range.

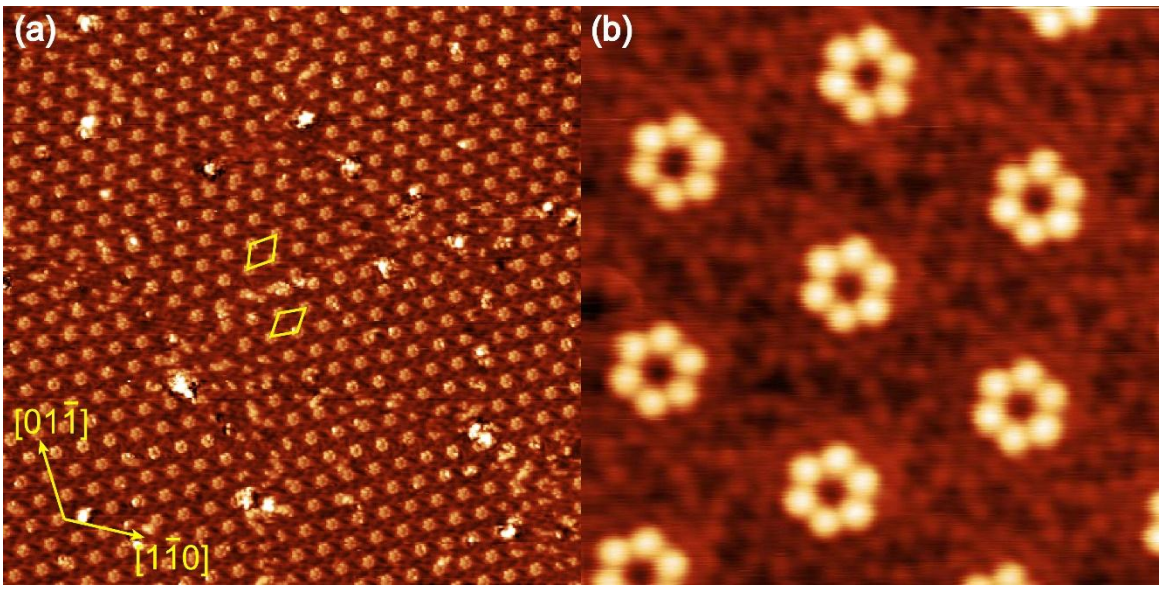

Fig. 1: STM images of 0.9±0.1 ML Ge deposited on Ag(111) at 455 K, acquired at 300 K after growth.

(a) 67 × 67 nm^2, Vbias = 1.7 V, I = 20 pA. (b) 8.5 × 8.5 nm^2, Vbias = -0.4 V, I = 2 nA. The unit cells of the two domains are indicated by yellow parallelograms.

Below 400 K, we obtained a surface where the protrusions are disordered. Above 460 K, the density of protrusions decreases and no ordered reconstruction is obtained. We didn't manage to obtain the $\left(7\sqrt{7} \times 7\sqrt{7}\right)$ reconstruction by evaporation, as the temperature on the STM was limited to 520 K. Fig. 1b shows a high resolution STM image of the reconstruction. In spite of the p3m1 symmetry of the substrate, the apparent space group of the surface reconstruction is clearly p6. The 6 protrusions per unit cell appear ~0.08 nm above the average height of the rest of the surface.

To gain more insight into the periodicity of the surface reconstruction, in-plane diffraction maps of the surface were obtained using surface X-ray diffraction (SXRD) at 300K, as shown in Figure 2a, after evaporation of 0.85±0.05 ML of Ge at 420 K. In addition to the intense spots at the node of the primitive unit cell of the Ag(111) surface, a high density of less intense spots is visible. They can be indexed on the basis of a $\left(\sqrt{109} \times \sqrt{109}\right)R \pm 24.5°$ reconstruction. This structure, with two possible domain orientations and with a lattice parameter of 3.02 nm, corresponds thus perfectly to the structure observed by STM. From the measured in-plane structure factors, we have computed the 2D Patterson map for the $\left(\sqrt{109} \times \sqrt{109}\right)R - 24.5°$ orientation, shown in Figure 2c, which is given by:[37] $P(x,y) = 2\sum_{HK}|F(H,K)|^2 \cos\left(2\pi(Hx + Ky)\right)$, where the (H,K,L) indices refer to the $\left(\sqrt{109} \times \sqrt{109}\right)$ basis and $F(H,K)$ are the structure factors specific of this reconstruction, and measured for $L = 0.11$. This Patterson map, an approximation of the electron density autocorrelation function, displays a complex pattern.

For comparison, we show in Fig. 2d the Patterson map obtained for honeycomb germanene, corresponding to the matching between the $\left(\sqrt{52} \times \sqrt{52}\right)$ and $\left(\sqrt{109} \times \sqrt{109}\right)$ unit cells of germanene and silver respectively. These two maps differ markedly, showing that the reconstruction observed is much more complex than any honeycomb layer.

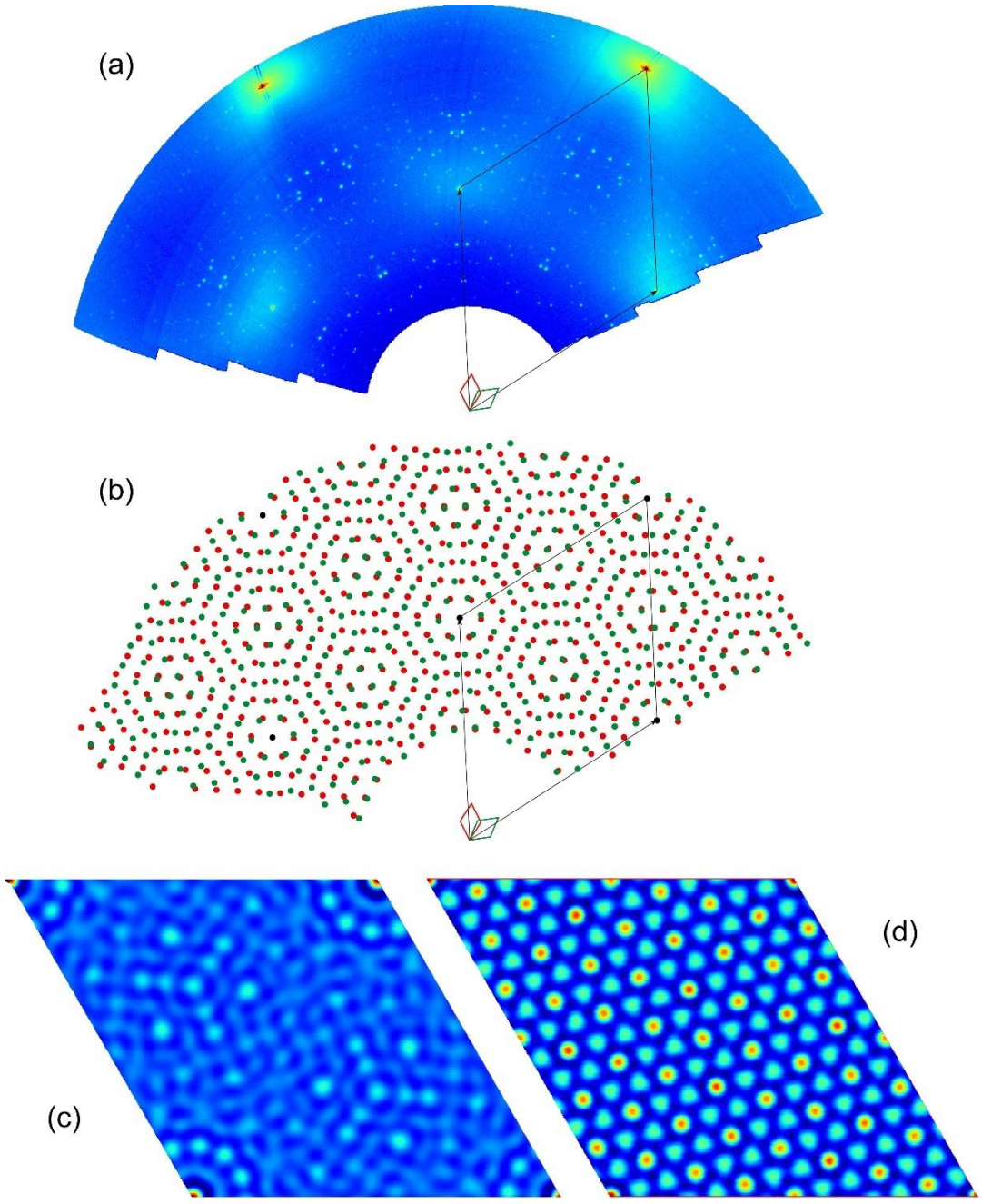

Fig. 2: (a) Diffracted intensity for in-plane conditions (L = 0.11) after evaporation of $\theta_{Ge} \approx 1$ ML on Ag(111) at T = 420 K. (b) Schematic of the diffraction pattern. The black parallelogram corresponds to the Ag(111) surface unit cell. The red and green parallelograms correspond to the $\left(\sqrt{109} \times \sqrt{109}\right)R \pm 24.5°$ supercells. (c) Experimental Patterson map of the $\left(\sqrt{109} \times \sqrt{109}\right)R - 24.5°$ structure. (d) Theoretical Patterson map of honeycomb germanene.

In order to determine the atomic structure of the $(\sqrt{109} \times \sqrt{109})$ reconstruction, it is not possible to explore *a priori* all possible models, due to the large number of atoms expected in the unit cell (more than 100 in the first layer). We have first determined the in-plane positions of the atoms in the surface layer by assuming a p6 symmetry as suggested from both SXRD and STM observations. For this purpose, we have used an iterative method to obtain the projected charge density from the in-plane structure factors.[38] The procedure is described in detail in the supporting information (SI). For the first estimate of the charge density, we have used the positions of the 54 protrusions per unit cell observed on STM images, assuming that they correspond to Ge atoms (see Fig. S1). After three iterations of the procedure, we obtained the configuration shown in Fig. 3a. It corresponds to a $Ge_{98}Ag_6$ layer, organized in hexagons, pentagons and heptagons. The agreement with the in-plane structure factors, shown in Fig. 3b, is excellent. In a second step, we have fitted the whole set of structure factors, i.e. in-plane and out-of-plane structure factors. For this purpose, we have added the Ag(111) substrate to the $Ge_{98}Ag_6$ layer and allowed all atoms of the $Ge_{98}Ag_6$ layer and first three substrate layers to move along in-plane and out-of-plane directions, taking into account a p3 space group for the system (see SI for details of the procedure). We obtained a perfect fit of the data with the fitted model of $Ge_{98}Ag_6$/Ag(111), corresponding to a reduced chi-squared $\chi^2 = 1.5$. The impressive comparison between experimental and simulated structure factors is shown in Fig. S2. As can be seen, all the

variations of the structure factor amplitude along the 397 reconstruction rods analyzed are nicely reproduced.

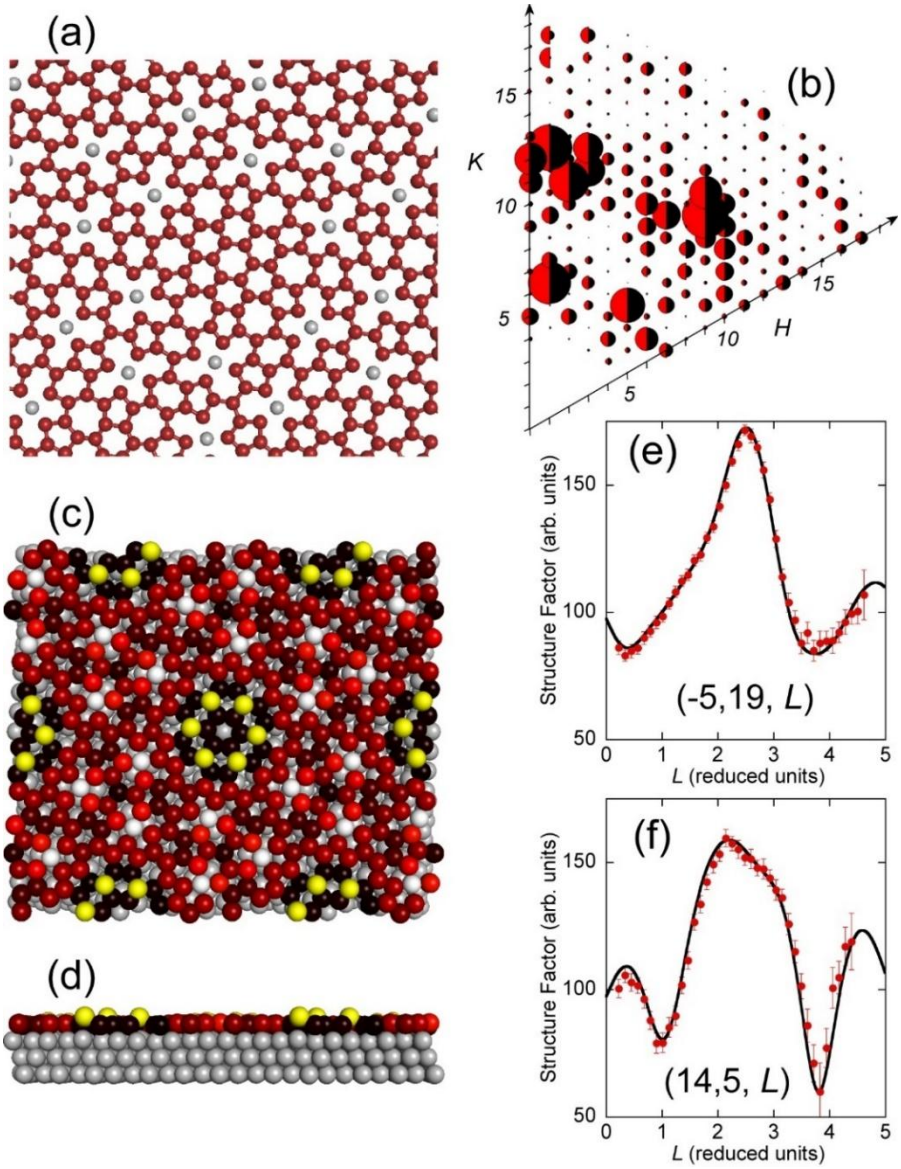

Fig. 3. (a) Top view of the $Ge_{98}Ag_6$ model of the $(\sqrt{109} \times \sqrt{109})$ reconstruction. (b) Corresponding non-equivalent in-plane structure factors, assuming a p6 symmetry. The measured and simulated structure factor amplitudes are shown by the radius of the red and black half disks respectively. (c-d) Top and side view of the $Ge_{98}Ag_6$/Ag(111) fitted model. Ge atoms

are colored from dark red to yellow according to their height, Ag surface atoms are colored in light grey. (e-f) Comparison between experimental (red dots) and simulated (black line) structure factors along the (-5,19, *L*) and (14, 5, *L*) rods respectively.

The fitted atomic structure is shown in Fig. 3c. In the $Ge_{98}Ag_6$ layer, 6 Ge atoms (in yellow) per unit cell sit at a higher distance (0.341 nm) from the average Ag(111) plane position than the other Ge atoms that are located between 0.216 nm and 0.257 nm above the Ag(111) plane. These 6 Ge atoms correspond to the hexamer pattern seen on STM images and the height difference between these 6 atoms and the other Ge atoms of the surface is very close to the value measured on STM images. As for the other Ge atoms, the highest ones (colored in light red) correspond also to the other protrusions seen on STM images. Fig. 3(e-f) shows the comparison of the structure factor amplitude along the (-5,19, *L*) and (14, 5, *L*) rods, which are equivalent for a 6-fold symmetry, but not equivalent for a 3-fold symmetry. They strongly differ, for $L \neq 0$, which shows the importance of substrate relaxations as only the substrate layers display a 3-fold symmetry instead of a 6-fold one. Indeed, sharp variations along the reconstruction rods, for example at *L=1* or *L=3.8* along the (14, 5, *L*) rod shown in Fig. 3f, are the signature of the elastic relaxations penetrating into the substrate.[39,40]

We have also fitted other configurations obtained by changing the chemical nature of atoms of the first two layers, resulting in 39 non-equivalent configurations. We have always obtained a worse agreement than the one obtained for $Ge_{98}Ag_6$/Ag(111) ($\chi^2 = 1.5$). Among those alternative configurations, the best agreement correspond to a pure germanium surface layer, i.e. Ge_{104}/Ag(111), with $\chi^2 = 3.1$ and to a two-layer surface alloy such as the one observed for Ge/Al(111),[21] i.e. $Ge_{98}Ag_6/Ge_6Ag_{103}$/Ag(111), with $\chi^2 = 2.7$.

We have then used DFT calculations to relax the $Ge_{98}Ag_6$/Ag(111) structure derived from the SXRD measurements and these two alternative structures. For comparison purpose, we have also relaxed two honeycomb models. The first one corresponds to the matching between $(\sqrt{52} \times \sqrt{52})$ and $(\sqrt{109} \times \sqrt{109})$ unit cells of germanene and silver respectively, whereas the second one, corresponds to the matching between $(3\sqrt{3} \times 3\sqrt{3})$ and (7×7) unit cells of germanene and silver respectively, i.e., to the model of germanene proposed by Yuhara et al.[34].

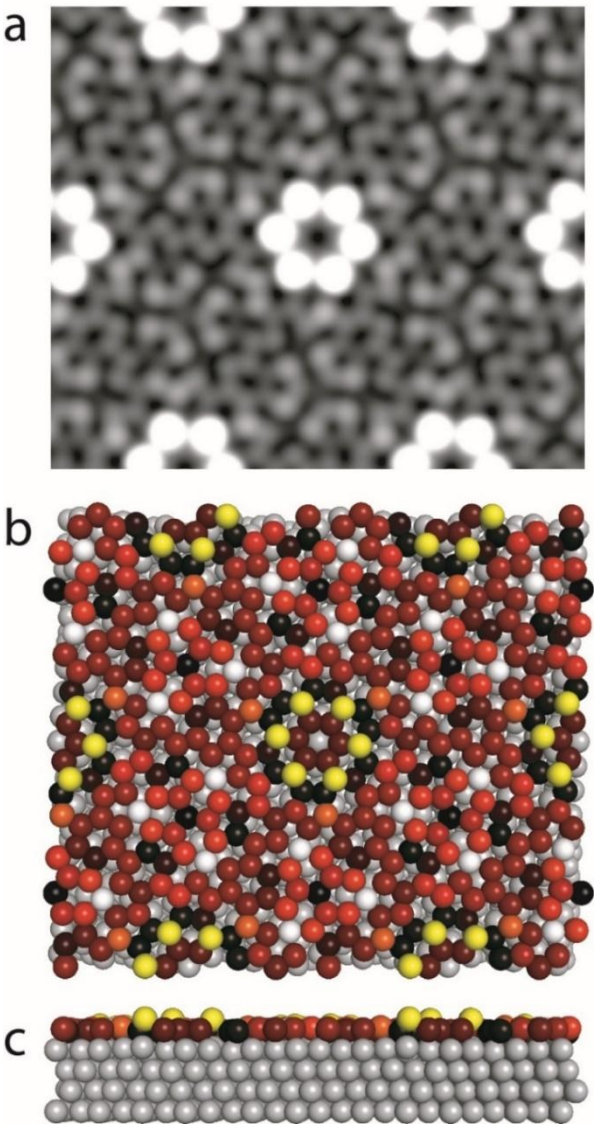

Fig. 4. (a) LDOS image of the $Ge_{98}Ag_6$/Ag(111) model relaxed by DFT, taken between $E_i = -0.4$ eV and $E_f = 0$ eV. (b-c) top and side view of the corresponding atomic structure. Ge atoms are colored from dark red to yellow according to their height, Ag surface atoms are colored in light grey.

The relaxed structure for the first model is displayed in Figs. 4b and 4c, while the structure for the other models are presented in the SI (Fig S3). There are 6 protruding Ge atoms per unit cell, lying at a distance of 0.355 nm above the Ag surface, while for the other Ge atoms, the distance to the Ag surface is in the 0.216-0.269 nm range. In other words, the structure derived from the DFT calculations is quite close to that obtained from the SXRD measurements. In the first layer, the root mean square (rms) displacements between SXRD and DFT positions is of 0.01nm only. Fig. 4 indicates that every protruding Ge is located above a Ag atom from the substrate; it appears that the latter lies at 0.027 nm higher than the other Ag atoms of the first Ag(111) plane. DFT calculations indicate that Ge-Ag distances are in the 0.265 – 0.288 nm range, and that the mean bond length between a protruding Ge and another Ge is equal to 0.257 nm, while being in the 0.248 – 0.257 nm range for the other Ge-Ge bonds. Since the atomic structure does not correspond to a honeycomb lattice, various bond angles are measured. The Ge-Ge-Ge angle is equal to 120° for the central hexagon in the flower motifs. It is equal to 95° for the protruding Ge atoms, and varies between 91° and 140° for the other Ge-Ge-Ge angles. On average, the value found is equal to 115°, which is very close to the one of freestanding germanene (113°). This justifies the extension of the Xene concept to the present layer. Finally, the Ge-Ag-Ge bond angles are in the 83°-96° range. Indeed, it can be seen in Fig. 4 that every Ag atom in the $Ge_{98}Ag_6$ layer is surrounded by four Ge atoms almost forming a square. Very similar parameters

have been obtained from the fit of the SXRD data. The detailed comparison is given in Table 1 in the SI.

Fig. 4a displays a local density of states (LDOS) image of the $Ge_{98}Ag_6$/Ag(111) system for energies between -0.4 and 0.0 eV. The comparison between the experimental STM image and the LDOS for all computed models is shown in Fig. S3. It can be seen that the calculated image in Fig. 4a is very close to the experimental STM image of Fig. 1. (see Fig. S3 for direct comparison). In particular the flower pattern is properly reproduced. The groups of 6 atoms (indicated by a red circle in Fig. S3 a,b) around each threefold rotation axis are also well reproduced. All atoms that are visible in the STM image are visible in the theoretical LDOS image. On the contrary, the agreement is less good with the Ge_{104}/Ag(111) and $Ge_{98}Ag_6/Ge_6Ag_{103}$/Ag(111) structures. Although the LDOS of these structures present the same flower patterns, they also exhibit bright spots, forming a hexagon around the hexamers, that are not visible in the experimental image. The honeycomb model of the $\left(\sqrt{109} \times \sqrt{109}\right)$ reconstruction (Fig. S3k) displays a completely different pattern. Thus, only the LDOS image for the $Ge_{98}Ag_6$/Ag(111) model is in agreement with our STM measurements. Note that the LDOS computed from the honeycomb model proposed by Yuhara et al. does not give a good agreement with their STM images (see Fig. S3e).

Eventually, we have compared the thermodynamical stability of the different models studied.

We present in Fig. 5 the formation energy of the various $\left(\sqrt{109} \times \sqrt{109}\right)$ models relaxed by DFT, as a function of $\Delta\mu_{\mathrm{Ge}}$, that is the deviation of μ_{Ge} with respect to $E_{\mathrm{Ge\,bulk}}$. Even if the chemical potential μ_{Ge} of the Ge atoms during growth is unknown, we expect that it becomes close to the one of bulk Ge at the completion of the $(\sqrt{109} \times \sqrt{109})$ reconstruction. This is

demonstrated by the coexistence of the $(\sqrt{109} \times \sqrt{109})$ reconstruction and 3D Ge islands observed for larger Ge coverage (See Fig. S4).

The formation energy γ is calculated as follows:

$$\gamma = \left(E_{\mathrm{Ge-Ag}} - E_{\mathrm{back-side\ Ag}} - N_{\mathrm{Ge}}\mu_{\mathrm{Ge}} - N_{\mathrm{Ag}}E_{\mathrm{Ag\ bulk}}\right)/A \qquad (1)$$

where $E_{\mathrm{Ge-Ag}}$ is the total energy of the considered model, N_{Ag} is the number of Ag atoms in the slab, while A is the area of the $(\sqrt{109} \times \sqrt{109})$ Ag(111) surface mesh. $E_{\mathrm{back-side\ Ag}}$ is the surface energy of the back-side of the Ag slab:

$$E_{\mathrm{back-side\ Ag}} = \left(E_{\mathrm{bare\ Ag}} - N_{\mathrm{Ag}}E_{\mathrm{Ag\ bulk}}\right)/2 \qquad (2)$$

where $E_{\mathrm{bare\ Ag}}$ is the energy of the bare Ag slab, formed of 4 layers of 109 atoms, and which exhibits two faces. A similar computation has been done for the (7×7) reconstruction.

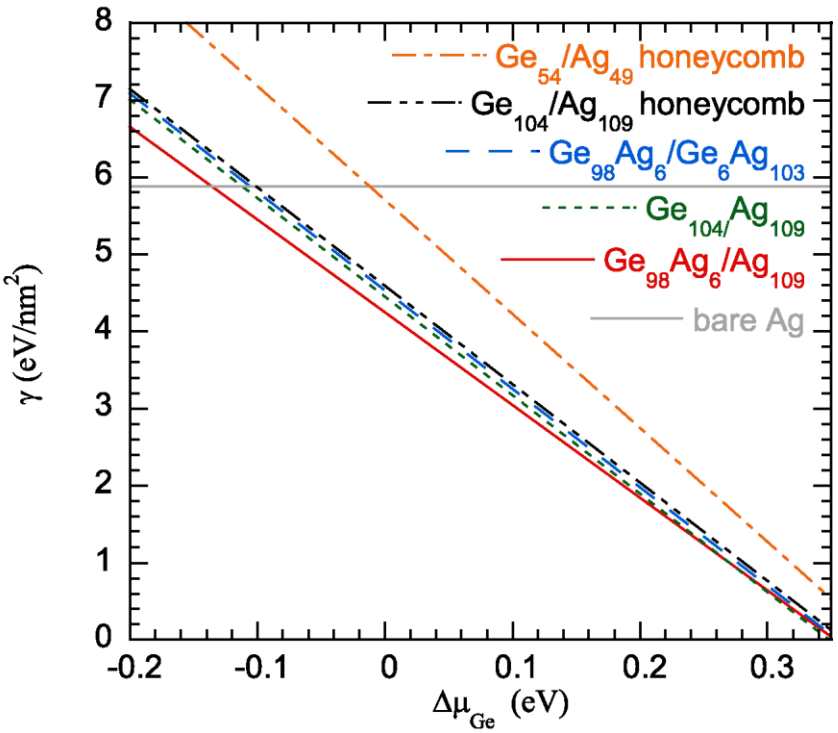

Figure 5: Formation energy as a function of $\Delta\mu_{Ge} = \mu_{Ge} - E_{Ge\,bulk}$ for the models of $(\sqrt{109} \times \sqrt{109})$ and (7×7) reconstructions. Continuous gray line: bare Ag(111) surface; red continuous line: $Ge_{98}Ag_6$/Ag(111); green dotted line: Ge_{104}/Ag(111). Blue dashed line: $Ge_{98}Ag_6/Ge_6Ag_{103}$/Ag(111); black dash-dotted line: Ge_{104}/Ag(111) honeycomb structure, orange dash-dot-dot line: Ge_{54}/Ag(111) honeycomb structure relaxed from the model of Yuhara et al.[34]

The most favorable system corresponds to $Ge_{98}Ag_6$/Ag(111) (red continuous line), for $\Delta\mu_{Ge}$ varying from -0.14 eV to 0.27 eV. Below -0.14 eV, the bare surface is preferred, while above 0.27 eV, the Ge_{104}/Ag(111) model (green dotted line) is preferred. The formation energies computed for honeycomb models are always higher.

Therefore, experiments and simulations demonstrate that the $\left(\sqrt{109} \times \sqrt{109}\right)R24.5°$ reconstruction observed after deposition of ~1 ML Ge on Ag(111) at 455 K corresponds to a $Ge_{98}Ag_6$ layer where atoms are organized in pentagons, hexagons and heptagons. There is a very good agreement between the atomic structure derived from the fit of the SXRD data and the one relaxed by DFT. The comparison with nearby models, corresponding to either pure germanene surface layers with similar or honeycomb structure or to alloyed bilayers ($Ge_{98}Ag_6/Ge_6Ag_{103}$) shows that the $Ge_{98}Ag_6$ model is energetically favored and much better reproduces the STM observations.

One may wonder if this structure presents some similarities with the one obtained by the segregation method by Yuhara et al.[34] Indeed, after 750 K annealing of a thick Ag/Ge(111) film, they obtained a surface entirely covered by a $\left(7\sqrt{7} \times 7\sqrt{7}\right)R19.1°$ reconstruction composed of one hexamer and three dimers per unit cell. Fig. 6a shows the corresponding LEED pattern they acquired. Apart from the spots corresponding to Ag(111), the most intense spots could be

assigned to a (1.35×1.35)R30° hexagonal lattice. This LEED pattern is very similar to the one we obtained after evaporation of $\theta_{Ge} \approx 1$ ML on Ag(111) at T = 420 K, shown in Fig. 6b. In this case, the most intense spots of the $\left(\sqrt{109} \times \sqrt{109}\right)R \pm 24.5°$ substrate reconstruction can be associated with a (1.38×1.38)R±29° hexagonal lattice. This shows the similarity of the local atomic arrangement between these two reconstructions. Fig. 6c shows the STM image obtained by Yuhara et al.[34] for the $\left(7\sqrt{7} \times 7\sqrt{7}\right)R19.1°$ reconstruction. We have mentioned above that this reconstruction cannot correspond to a $\left(3\sqrt{21} \times 3\sqrt{21}\right)R10.9°$ reconstruction of a germanene monolayer, as suggested by these authors since the coincidence cell would be smaller and equal to $(7 \times 7)_{Ag}$, that would coincide with $\left(3\sqrt{3} \times 3\sqrt{3}\right)R30°_{Ge}$. Moreover, the LDOS computed after relaxation of the honeycomb model proposed by Yuhara et al.[34] (see Fig. S3e) does not show any similarity with their STM observations. On the contrary, the $\left(7\sqrt{7} \times 7\sqrt{7}\right)R19.1°$ reconstruction presents many similarities with the $\left(\sqrt{109} \times \sqrt{109}\right)R24.5°$ one. Besides the motif of hexamers, which is clearly recognizable, and the dimers that appears as one third of a hexamer, other motifs are identical on both reconstructions such as the three-branches motif drawn in blue in Fig. 6. In the $\left(\sqrt{109} \times \sqrt{109}\right)R24.5°$ reconstruction, they correspond respectively to a Ge atom connected to 3 Ge pentagons. This suggest that the $\left(7\sqrt{7} \times 7\sqrt{7}\right)R19.1°$ should be also built with Ge pentagons, hexagons, heptagons and Ag atoms. Using these building blocks, we have searched for a possible atomic structure and we have constructed "by hand" the ball-and-stick model of a $Ge_{308}Ag_{24}$ layer, shown in Fig. 6. As can be seen, the protrusions seen in the STM images correspond nicely to the Ge atoms of the model.

A direct comparison of the two models is shown in Fig. S5, evidencing the similarity of the atomic structures. The atomic structure around the hexagons is identical. Both structures differ

by the presence of Ge dimers, derived from the hexamers by removing their central part, and by the larger density of pentagons for the $(7\sqrt{7} \times 7\sqrt{7})$ reconstruction. The Ag concentration in the surface layer is also slightly higher for the $(7\sqrt{7} \times 7\sqrt{7})$ reconstruction (7.2%) than for the $(\sqrt{109} \times \sqrt{109})$ reconstruction (5.8%). We attribute the small differences observed between the two reconstructions to the large difference of temperature during the preparation of the surface.

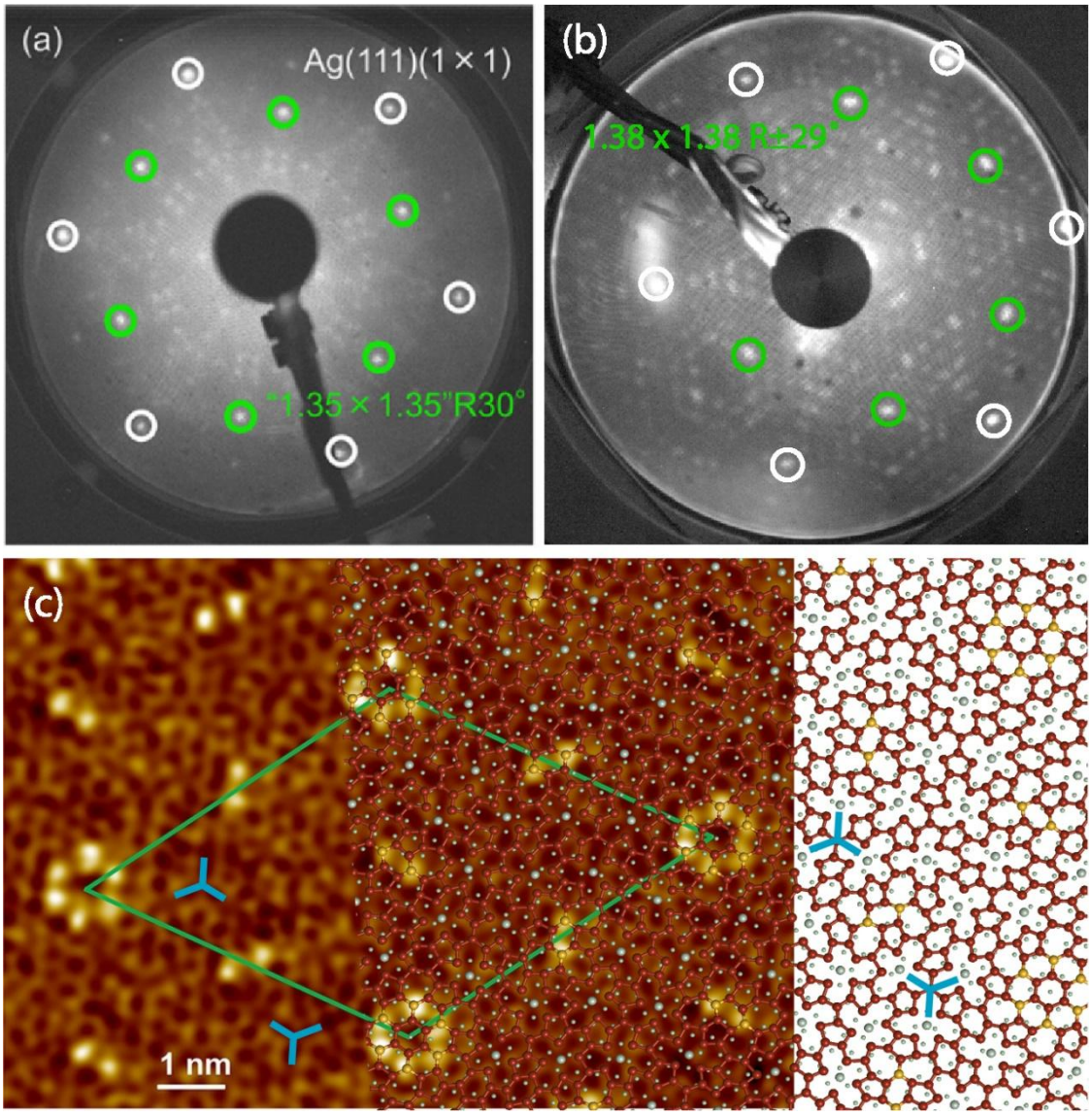

Fig. 6. a) LEED pattern (E = 63 eV) of an epitaxial Ag(111) thin film on Ge(111) after annealing et 753 K. (b) LEED pattern (E = 57 eV) obtained after evaporation of $\theta_{Ge} \approx 1$ ML on

Ag(111) at T = 420 K. c) Comparison between the STM image of germanene epitaxially grown on a Ag(111) thin film by the segregation method, from ref.[34] and the ball-and-stick model of $Ge_{308}Ag_{24}$ layer that we propose. Top Ge atoms are drawn in yellow, other Ge atoms in red, Ag atoms in grey. Ag atoms of the second plane are drawn with a smaller size. Some three-branches motifs are shown in blue. (a) and (c) adapted with permission from Yuhara et al. ACS Nano 2018, 12, 11, 11632-11637 doi:10.1021/acsnano.8b07006. Copyright 2018 American Chemical Society.

In conclusion, we have shown that the vacuum deposition of around one monolayer of Ge on Ag(111) results in the formation of a $\left(\sqrt{109} \times \sqrt{109}\right)R24.5°$ structure, with one hexamer of protrusions per unit cell. By using an original combination of STM and SXRD measurements, we have, at the atomic scale, completely determined the structure of this layer, which involves 104 surface atoms (98 Ge atoms and 6 Ag atoms), and is built with Ge pentagons, hexagons, heptagons and Ag atoms. The stability of this layer is confirmed by DFT calculations. We show that the protrusions seen by STM correspond to Ge atoms on top of Ag substrate atoms, and not to Ge adatoms above a Ag_2Ge or $AgGe_2$ surface alloy.[16,28,33] Thus, in contrast to the conclusion drawn by some of us in ref. [16], it appears that germanene can be grown on a Ag(111) substrate.

Interestingly, we show that the $\left(\sqrt{109} \times \sqrt{109}\right)R24.5°$ reconstruction is very similar to a previously observed structure, corresponding to a $\left(7\sqrt{7} \times 7\sqrt{7}\right)R19.1°$ surface reconstruction, obtained after segregation of Ge through a thick Ag/Ge(111) film, and formed by one hexamer and three dimers per unit cell. The latter was associated to honeycomb germanene by use of a ball-and-stick model.[34] However, the proposed model corresponds in reality to a smaller unit cell and is clearly to be rejected. This giant reconstruction, whose area is four time the one of the

(7×7) reconstruction of Si(111), was thus destined to remain misunderstood for a long time, because its size was too large to be determined by DFT methods. By analogy with the obtained atomic structure of the $\left(\sqrt{109} \times \sqrt{109}\right)$ reconstruction, we have been then able to determine the atomic structure of the $\left(7\sqrt{7} \times 7\sqrt{7}\right)$ reconstruction, which involves as much as 332 surface atoms. Beyond the challenge of solving such large structures, never done before, we finally show that the ground state of a germanene layer on Ag(111) is not a honeycomb Ge structure, but a complex organization of Ge pentagons, hexagons and heptagons, with a small quantity of Ag atoms.

Our result opens new perspectives related to the understanding of the complex structures observed after growth of Ge or Si on metal surfaces, such as the $\left(\sqrt{19} \times \sqrt{19}\right)$ reconstruction of Ge/Pt(111),[5] or the various reconstructions observed for Si/Au(111),[41] that have been initially described as silicene or germanene honeycomb layers.

METHODS

STM experiments have been performed in an ultra-high vacuum (UHV) system with a base pressure less than 1×10^{-10} mbar equipped with an Omicron variable temperature STM. The Ag(111) single crystal was prepared by several cycles of Ar ion sputtering ($P = 7\times10^{-5}$ mbar, 600 eV) and annealing ($T = 870$ K). Germanium was evaporated from a graphite crucible using a Focus GMBH e-beam evaporator installed in front of the STM with a flux $F \approx 0.16$ ML/h, where 1 ML corresponds to a germanene layer. All coverages have been calibrated using the completion of the striped phase as a reference,[29] associated with a Ge atomic density of 4.91 10^{14}

at/cm^2, or 0.335 ML. All STM images presented here have been acquired at room temperature after growth. The absence of oxygen and carbon contamination has been checked after growth by Auger Electron Spectroscopy (AES) (see Fig. S6).

SXRD experiments were performed at the SIXS beamline of SOLEIL synchrotron. The Ag(111) sample was prepared in a similar way as for STM experiments. Ge was evaporated in the diffraction chamber from a crucible using a Knudsen cell with a sample kept at ~ 420 K with a flux of 0.44 ML/h. After evaporation, the sample was analyzed at room temperature with 18.46 keV X-rays at a grazing incidence angle of 0.2°. Scattered X-rays were detected with a 2D detector in continuous acquisition mode, and the detector was kept in its best dynamic range by constantly adapting the beam attenuation.[42] Diffracted intensity was measured by performing a series of wide rocking scans for various values of the in-plane and out-of-plane momentum transfers. We used the "BINoculars" software to produce three-dimensional (3D) intensity data in the reciprocal space from the raw data[43]. The intensity was further integrated along the direction parallel to the surface to obtain the structure factors.[44] For this purpose, the data were fitted with the product of a lorentzian lineshape in one direction with a gaussian lineshape convolved with a square wave in the other direction, using a home-made software, and the fitted function has been analytically integrated (details are given in the SI). We finally obtained a set of 404 non-equivalent in-plane structure factors and a set of 15154 structure factors along 397 inequivalent reconstruction rods. The (H, K, L) indices used for indexing a reflection in reciprocal space refer to the Ag(111) $-(\sqrt{109} \times \sqrt{109})$ reconstruction basis ($a = b = 3.0157$ nm, $c = 0.7075$ nm, $\alpha = \beta = 90°, \gamma = 120°$).

The calculations have been carried on with the VASP (Vienna Ab initio simulation package) code[45–48] with the projector augmented-wave (PAW) method,[49,50] within the GGA approximation. The PBE (Perdew, Burke and Ernzerhof) functional has been used,[51,52] and the van der Waals interactions have been taken into account using the D2 correction of Grimme, due to the large size of the unit cell.[53,54] The plane wave cut-off energy is 450 eV, and the models are relaxed until the final atomic forces are lower than 0.2 eV.nm^{-1}. The surface unit cell corresponds to a $(\sqrt{109} \times \sqrt{109})$ mesh with respect to the Ag(111) substrate, and the calculation slab consists of three layers of 109 Ag atoms, one layer of 109 atoms (only Ag atoms or Ag and Ge atoms), and one adsorbate layer of pure Ge or a mixing of Ge and Ag atoms, containing 104 atoms. As a result, the supercell contains 540 atoms, and the slab size is (3.064 × 3.064 × 2.7 nm^3). The bottom Ag layer is kept fixed during calculations, and the Brillouin zone is described by (1×1×1) k-points. The optimized Ag lattice constant is 0.4150 nm (while the experimental one is 0.4085 nm). The local density of states (LDOS) images have been carried on within the Tersoff Hamann approximation.[55].

ASSOCIATED CONTENT

Supporting Information.

The Supporting Information is available free of charge on the ACS Publications website at DOI:

Details of the procedure used for determining the atomic positions from the experimental structure factors; comparison between experimental and theoretical structure factors corresponding to the model shown in Fig. 3c,d; comparison between atomic structure and LDOS

of the different models relaxed by DFT; comparison of the structural parameters for the $Ge_{98}Ag_6/Ag_{109}$ model determined by DFT or from SXRD; STM image of a 3D Ge island next to the $\left(\sqrt{109} \times \sqrt{109}\right)R24.5°$ reconstruction; comparison between the atomic structure of the $\left(7\sqrt{7} \times 7\sqrt{7}\right)R19.1°$ and $\left(\sqrt{109} \times \sqrt{109}\right)R24.5°$ reconstructions; AES spectrum of the surface after Ge evaporation.

AUTHOR INFORMATION

Corresponding Author

*email: prevot@insp.jussieu.fr

Author Contributions

The manuscript was written through contributions of all authors. All authors have given approval to the final version of the manuscript. All authors contributed equally.

Funding Sources

This study is financially supported the French National Research Agency (Germanene project ANR-17-CE09-0021-03). K.Z. is supported by the Chinese Scholarship Council (CSC contract 201808070070). The authors would like to acknowledge the High Performance Computing Center of the University of Strasbourg for supporting this work by providing scientific support and access to computing resources. Part of the computing resources were funded by the Equipex Equip@Meso project (Programme Investissements d'Avenir) and the CPER Alsacalcul/Big Data.

REFERENCES

(1) Molle, A.; Goldberger, J.; Houssa, M.; Xu, Y.; Zhang, S.-C.; Akinwande, D. Buckled Two-Dimensional Xene Sheets. *Nature Materials* **2017**, *16* (2), 163–169. https://doi.org/10.1038/nmat4802.

(2) Masson, L.; Prévot, G. Epitaxial Growth and Structural Properties of Silicene and Other 2D Allotropes of Si. *Nanoscale Adv.* **2023**, *5* (6), 1574–1599. https://doi.org/10.1039/D2NA00808D.

(3) Liu, C.-C.; Feng, W.; Yao, Y. Quantum Spin Hall Effect in Silicene and Two-Dimensional Germanium. *Physical Review Letters* **2011**, *107* (7), 076802. https://doi.org/10.1103/PhysRevLett.107.076802.

(4) Bechstedt, F.; Gori, P.; Pulci, O. Beyond Graphene: Clean, Hydrogenated and Halogenated Silicene, Germanene, Stanene, and Plumbene. *Progress in Surface Science* **2021**, *96* (3), 100615. https://doi.org/10.1016/j.progsurf.2021.100615.

(5) Li, L.; Lu, S.; Pan, J.; Qin, Z.; Wang, Y.; Wang, Y.; Cao, G.; Du, S.; Gao, H.-J. Buckled Germanene Formation on Pt(111). *Advanced Materials* **2014**, *26* (28), 4820–4824. https://doi.org/10.1002/adma.201400909.

(6) Bampoulis, P.; Zhang, L.; Safaei, A.; van Gastel, R.; Poelsema, B.; Zandvliet, H. J. W. Germanene Termination of Ge $_2$ Pt Crystals on Ge(110). *Journal of Physics: Condensed Matter* **2014**, *26* (44), 442001. https://doi.org/10.1088/0953-8984/26/44/442001.

(7) Dávila, M. E.; Xian, L.; Cahangirov, S.; Rubio, A.; Le Lay, G. Germanene: A Novel Two-Dimensional Germanium Allotrope Akin to Graphene and Silicene. *New Journal of Physics* **2014**, *16* (9), 095002. https://doi.org/10.1088/1367-2630/16/9/095002.

(8) Derivaz, M.; Dentel, D.; Stephan, R.; Hanf, M.-C.; Mehdaoui, A.; Sonnet, P.; Pirri, C. Continuous Germanene Layer on Al(111). *Nano Letters* **2015**, *15* (4), 2510–2516. https://doi.org/10.1021/acs.nanolett.5b00085.

(9) Zhang, L.; Bampoulis, P.; Rudenko, A. N.; Yao, Q.; van Houselt, A.; Poelsema, B.; Katsnelson, M. I.; Zandvliet, H. J. W. Structural and Electronic Properties of Germanene on MoS 2. *Physical Review Letters* **2016**, *116* (25), 256804. https://doi.org/10.1103/PhysRevLett.116.256804.

(10) Persichetti, L.; Jardali, F.; Vach, H.; Sgarlata, A.; Berbezier, I.; De Crescenzi, M.; Balzarotti, A. Van Der Waals Heteroepitaxy of Germanene Islands on Graphite. *The Journal of Physical Chemistry Letters* **2016**, *7* (16), 3246–3251. https://doi.org/10.1021/acs.jpclett.6b01284.

(11) Gou, J.; Zhong, Q.; Sheng, S.; Li, W.; Cheng, P.; Li, H.; Chen, L.; Wu, K. Strained Monolayer Germanene with 1 × 1 Lattice on Sb(111). *2D Mater.* **2016**, *3* (4), 045005. https://doi.org/10.1088/2053-1583/3/4/045005.

(12) Qin, Z.; Pan, J.; Lu, S.; Shao, Y.; Wang, Y.; Du, S.; Gao, H.-J.; Cao, G. Direct Evidence of Dirac Signature in Bilayer Germanene Islands on Cu(111). *Advanced Materials* **2017**, *29* (13), 1606046. https://doi.org/10.1002/adma.201606046.

(13) Lin, C.-H.; Huang, A.; Pai, W. W.; Chen, W.-C.; Chen, T.-Y.; Chang, T.-R.; Yukawa, R.; Cheng, C.-M.; Mou, C.-Y.; Matsuda, I.; Chiang, T.-C.; Jeng, H.-T.; Tang, S.-J. Single-

Layer Dual Germanene Phases on Ag(111). *Physical Review Materials* **2018**, *2* (2), 024003. https://doi.org/10.1103/PhysRevMaterials.2.024003.
(14) Ho, C.-S.; Banerjee, S.; Batzill, M.; Beck, D. E.; Koel, B. E. Formation and Structure of a (√19×√19)R23.4°-Ge/Pt(111) Surface Alloy. *Surface Science* **2009**, *603* (9), 1161–1167. https://doi.org/10.1016/j.susc.2009.01.028.
(15) Oughaddou, H.; Sawaya, S.; Goniakowski, J.; Aufray, B.; Lay, G. L.; Gay, J. M.; Treglia, G.; Biberian, J. P.; Barrett, N.; Guillot, C.; Mayne, A.; Dujardin, G. Ge/Ag(111) Semiconductor-on-Metal Growth: Formation of an Ag2Ge Surface Alloy. *Physical Review B* **2000**, *62* (24), 16653–16656.
(16) Zhang, K.; Bernard, R.; Borensztein, Y.; Cruguel, H.; Prévot, G. Growth of Germanium-Silver Surface Alloys Followed by *in Situ* Scanning Tunneling Microscopy: Absence of Germanene Formation. *Physical Review B* **2020**, *102* (12), 125418. https://doi.org/10.1103/PhysRevB.102.125418.
(17) Muzychenko, D. A.; Oreshkin, A. I.; Oreshkin, S. I.; Ustavschikov, S. S.; Putilov, A. V.; Aladyshkin, A. Yu. The Surface Structures Growth's Features Caused by Ge Adsorption on the Au(111) Surface. *JETP Letters* **2017**, *106* (4), 217–222. https://doi.org/10.1134/S0021364017160111.
(18) Cantero, E. D.; Solis, L. M.; Tong, Y.; Fuhr, J. D.; Martiarena, M. L.; Grizzi, O.; Sánchez, E. A. Growth of Germanium on Au(111): Formation of Germanene or Intermixing of Au and Ge Atoms? *Phys. Chem. Chem. Phys.* **2017**, *19* (28), 18580–18586. https://doi.org/10.1039/C7CP02949G.
(19) Wang, W.; Uhrberg, R. I. G. Investigation of the Atomic and Electronic Structures of Highly Ordered Two-Dimensional Germanium on Au(111). *Physical Review Materials* **2017**, *1* (7), 074002. https://doi.org/10.1103/PhysRevMaterials.1.074002.
(20) Martínez, E. A.; Fuhr, J. D.; Grizzi, O.; Sánchez, E. A.; Cantero, E. D. Growth of Germanene on Al(111) Hindered by Surface Alloy Formation. *The Journal of Physical Chemistry C* **2019**, *123*, 12910–12918. https://doi.org/10.1021/acs.jpcc.9b02614.
(21) Zhang, K.; Sciacca, D.; Hanf, M.-C.; Bernard, R.; Borensztein, Y.; Resta, A.; Garreau, Y.; Vlad, A.; Coati, A.; Lefebvre, I.; Derivaz, M.; Pirri, C.; Sonnet, P.; Stephan, R.; Prévot, G. Structure of Germanene/Al(111): A Two-Layer Surface Alloy. *J. Phys. Chem. C* **2021**, *125* (44), 24702–24709. https://doi.org/10.1021/acs.jpcc.1c07585.
(22) Zhang, K.; Hanf, M.-C.; Sciacca, D.; Bernard, R.; Borensztein, Y.; Resta, A.; Garreau, Y.; Vlad, A.; Coati, A.; Lefebvre, I.; Derivaz, M.; Pirri, C.; Sonnet, P.; Stephan, R.; Prévot, G. Combined Surface X-Ray Diffraction and Density Functional Theory Study of the Germanene/Al(111)- (7 × 7) R 19 . 1 ∘ Structure. *Phys. Rev. B* **2022**, *106* (4), 045412. https://doi.org/10.1103/PhysRevB.106.045412.
(23) Peng, W.; Xu, T.; Diener, P.; Biadala, L.; Berthe, M.; Pi, X.; Borensztein, Y.; Curcella, A.; Bernard, R.; Prévot, G.; Grandidier, B. Resolving the Controversial Existence of Silicene and Germanene Nanosheets Grown on Graphite. *ACS Nano* **2018**, *12* (5), 4754–4760. https://doi.org/10.1021/acsnano.8b01467.
(24) Golias, E.; Xenogiannopoulou, E.; Tsoutsou, D.; Tsipas, P.; Giamini, S. A.; Dimoulas, A. Surface Electronic Bands of Submonolayer Ge on Ag(111). *Physical Review B* **2013**, *88* (7), 075403. https://doi.org/10.1103/PhysRevB.88.075403.
(25) Chiniwar, S.; Huang, A.; Chen, T.-Y.; Lin, C.-H.; Hsing, C.-R.; Chen, W.-C.; Cheng, C.-M.; Jeng, H.-T.; Wei, C. M.; Pai, W. W.; Tang, S.-J. Substrate-Mediated Umklapp

Scattering at the Incommensurate Interface of a Monatomic Alloy Layer. *Physical Review B* **2019**, *99* (15), 155408. https://doi.org/10.1103/PhysRevB.99.155408.
(26) Wang, W.; Sohail, H. M.; Osiecki, J. R.; Uhrberg, R. I. G. Broken Symmetry Induced Band Splitting in the Ag 2 Ge Surface Alloy on Ag(111). *Physical Review B* **2014**, *89* (12), 125410. https://doi.org/10.1103/PhysRevB.89.125410.
(27) Liu, Y.; Zhuang, J.; Liu, C.; Wang, J.; Xu, X.; Li, Z.; Zhong, J.; Du, Y. Role of Atomic Interaction in Electronic Hybridization in Two-Dimensional Ag_2Ge Nanosheets. *The Journal of Physical Chemistry C* **2017**, *121* (31), 16754–16760. https://doi.org/10.1021/acs.jpcc.7b02017.
(28) Zhuang, J.; Liu, C.; Zhou, Z.; Casillas, G.; Feng, H.; Xu, X.; Wang, J.; Hao, W.; Wang, X.; Dou, S. X.; Hu, Z.; Du, Y. Dirac Signature in Germanene on Semiconducting Substrate. *Advanced Science* **2018**, *5* (7), 1800207. https://doi.org/10.1002/advs.201800207.
(29) Zhang, K.; Sciacca, D.; Coati, A.; Bernard, R.; Borensztein, Y.; Diener, P.; Grandidier, B.; Lefebvre, I.; Derivaz, M.; Pirri, C.; Prévot, G. Resolving the Structure of the Striped Ge Layer on Ag(111): Ag2Ge Surface Alloy with Alternate Fcc and Hcp Domains. *Physical Review B* **2021**, *104* (15), 155403. https://doi.org/10.1103/PhysRevB.104.155403.
(30) Chen, T.-Y.; Mikolas, D.; Chiniwar, S.; Huang, A.; Lin, C.-H.; Cheng, C.-M.; Mou, C.-Y.; Jeng, H.-T.; Pai, W. W.; Tang, S.-J. Germanene Structure Enhancement by Adjacent Insoluble Domains of Lead. *Phys. Rev. Research* **2021**, *3* (3), 033138. https://doi.org/10.1103/PhysRevResearch.3.033138.
(31) Kesper, L.; Hochhaus, J. A.; Schmitz, M.; Schulte, M. G. H.; Berges, U.; Westphal, C. Tracing the Structural Evolution of Quasi-Freestanding Germanene on Ag(111). *Sci Rep* **2022**, *12* (1), 7559. https://doi.org/10.1038/s41598-022-10943-0.
(32) Oughaddou, H.; Mayne, A.; Aufray, B.; Bibérian, J. P.; Le Lay, G.; Ealet, B.; Dujardin, G.; Kara, A. Germanium Adsorption on Ag(111): An AES-LEED and STM Study. *Journal of Nanoscience and Nanotechnology* **2007**, *7* (9), 3189–3192. https://doi.org/10.1166/jnn.2007.677.
(33) Mu, H.; Liu, Y.; Bongu, S. R.; Bao, X.; Li, L.; Xiao, S.; Zhuang, J.; Liu, C.; Huang, Y.; Dong, Y.; Helmerson, K.; Wang, J.; Liu, G.; Du, Y.; Bao, Q. Germanium Nanosheets with Dirac Characteristics as a Saturable Absorber for Ultrafast Pulse Generation. *Adv. Mater.* **2021**, 2101042. https://doi.org/10.1002/adma.202101042.
(34) Yuhara, J.; Shimazu, H.; Ito, K.; Ohta, A.; Araidai, M.; Kurosawa, M.; Nakatake, M.; Le Lay, G. Germanene Epitaxial Growth by Segregation through Ag(111) Thin Films on Ge(111). *ACS Nano* **2018**, *12* (11), 11632–11637. https://doi.org/10.1021/acsnano.8b07006.
(35) Mizuno, S.; Ohta, A.; Suzuki, T.; Kageshima, H.; Yuhara, J.; Hibino, H. Correlation between Structures and Vibration Properties of Germanene Grown by Ge Segregation. *Appl. Phys. Express* **2021**, *14* (12), 125501. https://doi.org/10.35848/1882-0786/ac3185.
(36) Cahangirov, S.; Topsakal, M.; Aktürk, E.; Şahin, H.; Ciraci, S. Two- and One-Dimensional Honeycomb Structures of Silicon and Germanium. *Physical Review Letters* **2009**, *102* (23), 236804. https://doi.org/10.1103/PhysRevLett.102.236804.
(37) Feidenhans'l, R. Surface Structure Determination by X-Ray Diffraction. *Surface Science Reports* **1989**, *10* (3), 105–188. https://doi.org/10.1016/0167-5729(89)90002-2.
(38) Tajiri, H. Progress in Surface X-Ray Crystallography and the Phase Problem. *Japanese Journal of Applied Physics* **2020**, *59* (2), 020503. https://doi.org/10.7567/1347-4065/ab631e.

(39) Prévot, G.; Coati, A.; Croset, B.; Garreau, Y. Direct Observation of Elastic Displacement Modes by Grazing-Incidence X-Ray Diffraction. *J Appl Crystallogr* **2007**, *40* (5), 874–882. https://doi.org/10.1107/S0021889807034115.
(40) Prévot, G.; Steadman, P.; Ferrer, S. Determination of the Elastic Dipole at the Atomic Steps of Pt(977) from Surface x-Ray Diffraction. *Phys. Rev. B* **2003**, *67* (24), 245409. https://doi.org/10.1103/PhysRevB.67.245409.
(41) Jaroch, T.; Krawiec, M.; Zdyb, R. Layered Heterostructure of Planar and Buckled Phases of Silicene. *2D Mater.* **2021**, *8* (3), 035038. https://doi.org/10.1088/2053-1583/ac00fb.
(42) Dawiec, A.; Garreau, Y.; Bisou, J.; Hustache, S.; Kanoute, B.; Picca, F.; Renaud, G.; Coati, A. Real-Time Control of the Beam Attenuation with XPAD Hybrid Pixel Detector. *J. Inst.* **2016**, *11* (12), P12018–P12018. https://doi.org/10.1088/1748-0221/11/12/P12018.
(43) Roobol, S.; Onderwaater, W.; Drnec, J.; Felici, R.; Frenken, J. *BINoculars* : Data Reduction and Analysis Software for Two-Dimensional Detectors in Surface X-Ray Diffraction. *J Appl Crystallogr* **2015**, *48* (4), 1324–1329. https://doi.org/10.1107/S1600576715009607.
(44) Drnec, J.; Zhou, T.; Pintea, S.; Onderwaater, W.; Vlieg, E.; Renaud, G.; Felici, R. Integration Techniques for Surface X-Ray Diffraction Data Obtained with a Two-Dimensional Detector. *Journal of Applied Crystallography* **2014**, *47* (1), 365–377. https://doi.org/10.1107/S1600576713032342.
(45) Kresse, G. Ab Initio Molecular Dynamics for Liquid Metals. *Journal of Non-Crystalline Solids* **1995**, *192–193*, 222–229. https://doi.org/10.1016/0022-3093(95)00355-X.
(46) Kresse, G.; Hafner, J. *Ab Initio* Molecular-Dynamics Simulation of the Liquid-Metal–Amorphous-Semiconductor Transition in Germanium. *Phys. Rev. B* **1994**, *49* (20), 14251–14269. https://doi.org/10.1103/PhysRevB.49.14251.
(47) Kresse, G.; Furthmüller, J. Efficiency of Ab-Initio Total Energy Calculations for Metals and Semiconductors Using a Plane-Wave Basis Set. *Computational Materials Science* **1996**, *6* (1), 15–50. https://doi.org/10.1016/0927-0256(96)00008-0.
(48) Kresse, G.; Furthmüller, J. Efficient Iterative Schemes for *Ab Initio* Total-Energy Calculations Using a Plane-Wave Basis Set. *Phys. Rev. B* **1996**, *54* (16), 11169–11186. https://doi.org/10.1103/PhysRevB.54.11169.
(49) Blöchl, P. E. Projector Augmented-Wave Method. *Phys. Rev. B* **1994**, *50* (24), 17953–17979. https://doi.org/10.1103/PhysRevB.50.17953.
(50) Kresse, G.; Joubert, D. From Ultrasoft Pseudopotentials to the Projector Augmented-Wave Method. *Phys. Rev. B* **1999**, *59* (3), 1758–1775. https://doi.org/10.1103/PhysRevB.59.1758.
(51) Perdew, J. P.; Burke, K.; Ernzerhof, M. Generalized Gradient Approximation Made Simple. *Phys. Rev. Lett.* **1996**, *77* (18), 3865–3868. https://doi.org/10.1103/PhysRevLett.77.3865.
(52) Perdew, J. P.; Burke, K.; Ernzerhof, M. Generalized Gradient Approximation Made Simple [Phys. Rev. Lett. 77, 3865 (1996)]. *Phys. Rev. Lett.* **1997**, *78* (7), 1396–1396. https://doi.org/10.1103/PhysRevLett.78.1396.
(53) Grimme, S. Accurate Description of van Der Waals Complexes by Density Functional Theory Including Empirical Corrections. *J. Comput. Chem.* **2004**, *25* (12), 1463–1473. https://doi.org/10.1002/jcc.20078.
(54) Grimme, S. Semiempirical GGA- type density functional constructed with a long- range dispersion correction. *Journal of Computational Chemistry* **2006**, *27* (15), 1787–1799. https://doi.org/10.1002/jcc.20495.
(55) Tersoff, J.; Hamann, D. R. Theory and Application for the Scanning Tunneling Microscope. *Phys. Rev. Lett.* **1983**, *50* (25), 1998–2001. https://doi.org/10.1103/PhysRevLett.50.1998.